SOILS AND FOUNDATIONS Vol. 45, No. 4, 119–132, Aug. 2005
Japanese Geotechnical Society

PHENOMENOLOGICAL MODEL APPLIED TO INELASTIC RESPONSE OF SOIL-PILE INTERACTION SYSTEMS

NIKOS GEROLYMOS[i] and GEORGE GAZETAS[ii]

ABSTRACT

A dynamic nonlinear Winkler spring model, is developed for the seismic response of deep foundations. The model utilizes the phenomenological "BWGG" model (outlined in a companion paper), and it can treat the inelastic response of both the *soil* and the *pile*. The nonlinear reaction of the soil is modeled realistically by the BWGG interaction springs and dashpots, with due consideration to effects such as: separation (gapping) of the pile or caisson from the soil, radiation damping, and loss of strength due to pore-water pressure development. The modeling of pile inelasticity is also versatile, and can treat from well-reinforced to poorly-reinforced concrete sections. The necessity for the proposed model arises from the difficulty to predict the large-amplitude dynamic response of piles up to failure. The BWGG-Winkler model is validated through the results of in-situ monotonic and dynamic pile load tests. It is further utilized to study the nonlinear soil-pile interaction under lateral monotonic loading. The results of the model are compared with the venerable Broms (1964) theory for pile lateral capacity

Key words: cyclic lateral loading, monotonic loading separation/gapping, pile, radiation damping, soil and pile inelasticity, Winkler-type model (**IGC**: E4/H1)

INTRODUCTION

Dynamic pile-soil interaction involves complicated geometric and material nonlinearities such as soil and structural inelasticity, separation and gapping of the pile from the soil, loss of soil strength due to pore pressure development.

The general problem of a single pile embedded in a cohesionless and cohesive soil and subjected to lateral loading is sketched in Fig. 1. It is interesting to note that the apparent gapping in the case of a cohesive foundation soil not only influences the soil reaction but also affects strongly the pile-soil radiation damping in the dynamic case. The problem becomes much more difficult when inelastic structural response of the pile is involved. Figure 2 presents two experimental force-displacement loops corresponding to a poorly and a well-reinforced concrete structural element respectively, subjected to lateral loading and experiencing intense inelastic behavior (after Tassios et al., 1996; Priestley et al., 1996).

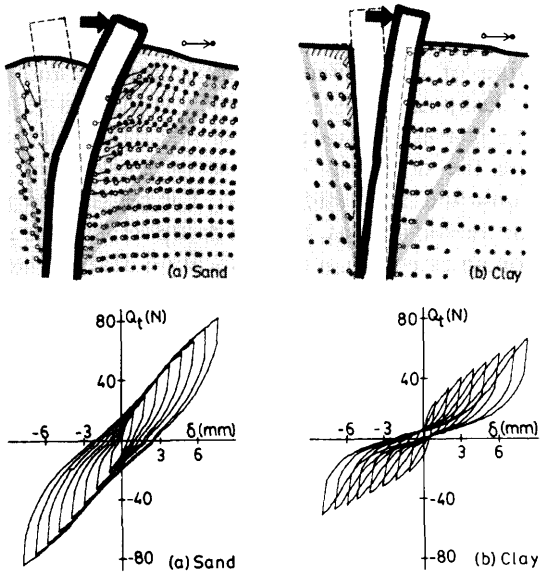

Fig. 1. The general problem of a single pile embedded in a cohesionless (left) and a cohesive (right) soil, and subjected to lateral loading (Kishida, 1985)

Trochanis et al. (1994) are the first to utilise the phenomenological hysteretic Bouc-Wen model in order to express the force-displacement relation of nonlinear springs distributed along the pile for approximating the lateral soil reaction. Their study focused on the static and cyclic response, and showed that the Bouc-Wen model was capable of describing the response of pile-soil systems. Badoni and Makris (1996) who also studied the lateral pile response utilised the nonlinear Bouc-Wen spring in conjuction with distributed viscous dashpots placed in parallel, as is appropriate for dynamic loading. The efficiency of their model was demonstrated against

[i] Post Ph.D. Researcher, National Technical University, Athens, Greece.
[ii] Professor, ditto. (gazetas@ath.forthnet.gr).
The manuscript for this paper was received for review on March 30, 2004; approved on May 30, 2005.
Written discussions on this paper should be submitted before March 1, 2006 to the Japanese Geotechnical Society, 4-38-2, Sengoku, Bunkyo-ku, Tokyo 112-0011, Japan. Upon request the closing date may be extended one month.

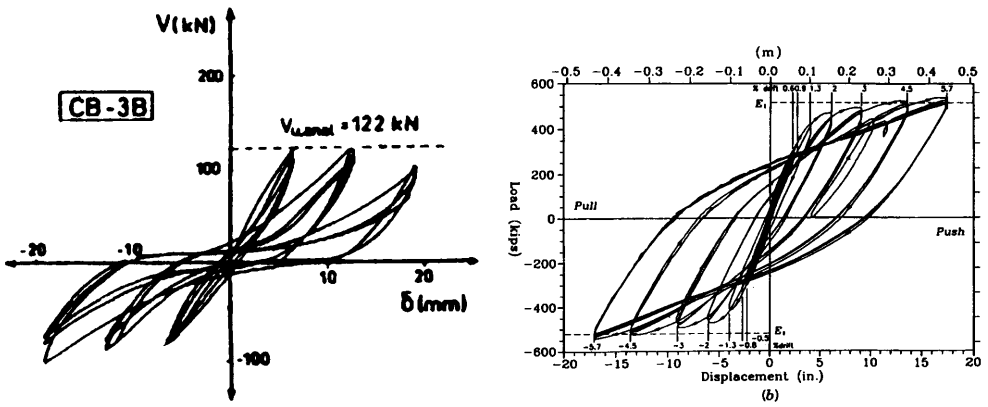

Fig. 2. Experimental force-displacement loops for a poorly reinforced (left-after Tassios et al.), and a well-reinforced (right-after Priestley et al.) concrete structural element

the experimentally measured single pile response. Although these Bouc-Wen type models were versatile in describing the soil-pile response, they had a number of limitations: (i) Neither pile nor soil-pile-interface nonlinearities were taken into consideration; (ii) the coupling between radiation damping and hysteretic soil response was ignored, and (iii) several features of the inelastic response of soil-pile systems, such as the stiffness and strength degradation with cyclic loading, could not be simulated.

In this paper a phenomenological Winkler-type model, consisting of distributed hysteretic springs and visco-plastic dashpots placed in parallel, is utilized to model both the lateral soil reaction and pile inelasticity and to compute the nonlinear response of single piles under monotonic and cyclic lateral load. The constitutive model used for the soil springs, the soil dashpots, and the pile, is based on an extension and modification of the Bouc-Wen model. The model is a system of mathematical expressions capable of fitting experimental data when its parameters are appropriately calibrated. It is not a physically motivated force-displacement constitutive law. This means that a comprehensive methodology for the identification/calibration of the model parameters shall be established. This could be achieved through the use of data: (i) from full-scale field experiments, (ii) from laboratory tests, (iii) from results of rigorous 3-D numerical analyses, and (iv) from results of centrifuge and shaking table tests. Advanced nonlinear optimization techniques could be utilized for this purpose. Although identification and complete calibration of the model parameters is not the prevailing task of this paper, a physically-motivated calibration procedure is developed so that many of the parameters of the proposed model are readily associated with understandable soil and pile properties, such as the Young's modulus of elasticity, the undrained shear strength (cohesive soil), the internal friction angle (cohesionless soil), the bending stiffness and the ultimate moment capacity of the pile cross-section.

The model is shown to be capable of reproducing complicated experimental behaviour with satisfactory engineering accuracy, and is subsequently used to compute the nonlinear response of a pile embedded in cohesionless soil when subjected to lateral monotonic loading. The results are compared with the venerable Broms (1964) theory for pile lateral capacity.

THE MODEL: EQUATIONS AND PARAMETERS

The constitutive relationship for the lateral soil reaction against a deflecting pile is expressed as the sum of an elastic and a hysteretic component according to:

$$F_s = \{\alpha_s k_x u + (1-\alpha_s) P_y \zeta_s\}(1-r_s) \tag{1}$$

in which F_s is the resultant in the direction of loading of the normal and shear stresses along the perimeter of the pile of a unit thickness, u is the lateral pile deflection at the location of the spring; k_x is the initial stiffness of the spring; α_s is a parameter that controls the post yielding stiffness, P_y is the ultimate soil reaction, r_s is a parameter that controls both strength and stiffness degradation of the soil reaction to cyclic loading, and ζ_s is an hysteretic dimensionless quantity that determines the nonlinear response of soil. The latter is governed by the following differential equation;

$$\frac{d\zeta_s}{dt} = \eta_s \frac{1}{u_y} \frac{A_s \frac{du}{dt} - b_s \frac{du}{dt} |\zeta_s|^{n_s} - g_s \left|\frac{du}{dt}\right| |\zeta_s|^{n_s-1}\zeta_s}{1 + \left[A_s - b_s |\zeta_s|^{n_s} - g_s \operatorname{sign}\left(\frac{du}{dt}\right) |\zeta_s|^{n_s-1}\zeta_s\right]\left\{L_s \exp\left[-\left(\frac{\zeta_s - \zeta_{s2}}{\zeta_{s1}}\right)^2\right]\right\}} \tag{2}$$

In the above equation A_s, b_s, g_s, n_s, η_s, L_s, ζ_{s1} and ζ_{s2} are dimensionless quantities which control the shape of the hysteretic soil-reaction-pile-deflection loop; u_y is the value of pile deflection at initiation of yielding in the soil. The exact role of each of these parameters will be illustrated in the sequel. Derivation of Eq. (2) is thoroughly explained in the companion paper "*Constitutive Model for 1-D Cyclic Soil Behaviour Applied to Seismic Analysis of Layered Deposits*" (Gerolymos and Gazetas, 2004), tentatively accepted for publication in Soils and Foundations.

The "damping" force resulting from the visco-plastic dashpot is given by;

$$F_d = c_x \frac{\partial u}{\partial t}\left[a_s + (1-a_s)\frac{\partial \zeta_s}{\partial u}\right]^{c_s} \tag{3}$$

where c_x is the damping coefficient at small amplitude motions, and c_s is a viscoplastic parameter which controls the coupling of soil and soil-pile interface nonlinearity with radiation damping.

The inelastic behaviour of the pile is expressed in terms of a strength-of-materials-type bending moment-pile curvature relation;

$$M = \left\{\alpha_p E_p I_p \frac{\partial^4 u}{\partial z^4} + (1-a_p) M_y \zeta_p\right\}(1-r_p) \tag{4}$$

where E_pI_p is the initial (elastic) bending stiffness (also called flexural rigidity), α_p is a parameter controlling the post yielding bending stiffness, M_y is the value of bending moment that initiates structure yielding in the pile, r_p is a parameter that controls both strength and stiffness degradation of the pile bending moment with cyclic loading, and ζ_p is the hysteretic dimensionless parameter which controls the nonlinear structural response of the pile. The latter is governed by the following differential equation;

$$\frac{d\zeta_p}{dt} = \eta_p \frac{1}{\kappa_y} \frac{A_p \frac{d\kappa}{dt} - b_p \frac{d\kappa}{dt}|\zeta_p|^{n_p} - g_p \left|\frac{d\kappa}{dt}\right| |\zeta_p|^{n_p-1}\zeta_p}{1 + \left[A_p - b_p|\zeta_p|^{n_p} - g_p \operatorname{sign}\left(\frac{d\kappa}{dt}\right)|\zeta_p|^{n_p-1}\zeta_p\right]\left\{L_p \exp\left[-\left(\frac{\zeta_p - \zeta_{p2}}{\zeta_{p1}}\right)^2\right]\right\}} \tag{5}$$

In the above equation, κ is the pile curvature, and A_p, b_p, g_p, n_p, η_p, L_p, ζ_{p1} and ζ_{p2} are dimensionless quantities that control the shape of the hysteretic bending moment-curvature loop. κ_y is the value of pile curvature at the initiation of pile yielding.

Evidently, Eqs. (4)-(5) are of the same form as Eqs. (1)-(2). More specifically Eqs. (1) and (2) relate the lateral soil reaction to the deflection of the pile, whereas Eqs. (4) and (5) relate the bending moment with the curvature at each point of the pile. These equations are a generalization and extension of a model originally proposed by Bouc (1971) and subsequently extended by Wen (1976), Baber and Wen (1981), and Baber and Noori (1985), and used in random vibrations studies of degrading-pinching inelastic systems. Similar expressions to those of Eqs. (2) and (3) have been previously used by Sivaselvan and Reinhorn (2000) to model the constitutive behavior of beam-column cross sections in structural analysis.

KEY PARAMETERS AND CAPABILITIES OF THE MODEL

In a companion paper by Gerolymos and Gazetas (2004), the authors have introduced the model as it relates to a τ-γ or σ-ε constitutive law. Therefore, only a brief outline is presented herein of the parameters, capabilities and limitations of the model.

Parameters for Monotonic Loading

The parameter n (n_s for soil reaction, and n_p for pile bending moment) controls the rate of transition from the elastic to the yield state. A large value of n (greater than 10) models approximately a bilinear hysteretic curve; decreasing values of n lead to smoother transitions where plastic behavior occurs even at low loading levels. Figure 3 illustrates the role n on the monotonic loading curve. The parameter α (α_s for soil reaction, and α_p for pile bending moment) is the ratio of post yielding to initial elastic stiffness. Monotonic loading curves for different values of the post yielding parameter α and for constant value of n are presented in Fig. 4. The parameters n and α can be properly calibrated to match: (a) any lateral "*p-y*" curve, such as those proposed by Reese (1974, 1975), and Matlock (1970) for sand, stiff and soft clay, as shown in Fig. 5, and (b) a variety of bending moment-curvature curves such as those obtained experimentally or numerically for a pile of reinforced concrete (Fig. 6).

Parameters for Unloading-Reloading

Parameters b (b_s for soil reaction, and b_p for pile bending moment) and g (g_s for soil reaction, and g_p for pile bending moment) control the shape of the unloading-reloading curve. As is shown in Fig. 7 there are four basic hysteretic shapes depending on the relation between b and g. When $b=g=0.5$, upon the stiffness reversal equals the initial stiffness, and hence the Masing criterion for loading-unloading-reloading is recovered. In the special case $b=1$ and $g=0$, the hysteretic loop collapses to the monotonic loading curve (nonlinear but elastic behavior).

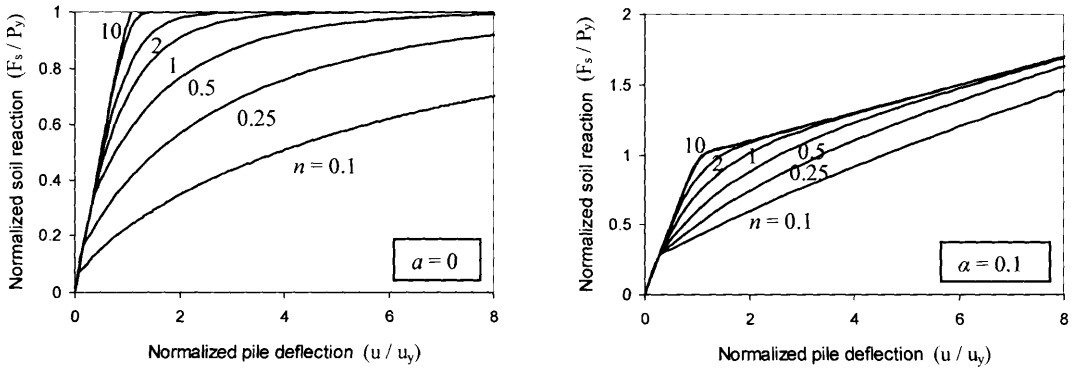

Fig. 3. Normalized soil reaction-pile deflection curves to monotonic loading for selected values of parameter n, computed with the proposed model for piles, $a=0$ and 0.1

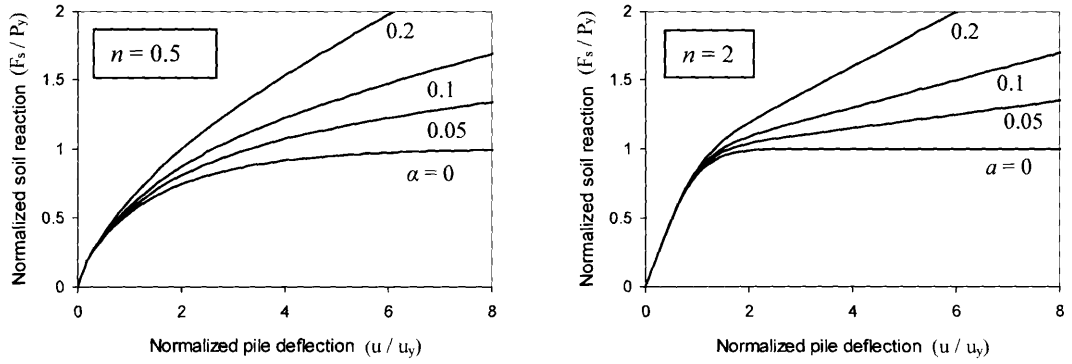

Fig. 4. Normalized soil reaction-pile deflection to monotonic loading for selected values of post-yielding parameter α computed with the proposed model for piles, $n=0.5$ and 2

Parameters for Stiffness and Strength Degradation with Cyclic Loading

The model is capable of reproducing stiffness and strength degrading behavior. Stiffness decay is controlled by the parameter η (η_s for soil, and η_p for pile). Prescribing η to be an increasing function of time will induce stiffness decay. η can be expressed as a function of the dissipated hysteretic energy and/or the cumulative displacement ductility. Its influence on the hysteretic loops is depicted in Fig. 8. It is evident that η affects only the tangent stiffness while the secant stiffness of the response remains constant.

The proposed model could also simulate strength degradation with cyclic loading. This can be achieved in two different ways: (i) By expressing parameters b and g to be increasing functions of the dissipated hysteretic energy and/or the cumulative displacement ductility; (ii) Both strength and stiffness degradation are controlled by parameter r (r_s for soil, and r_p for pile). Increasing r, is equivalent to reducing parameter A without affecting b and g. Parameter r can be prescribed as an increasing function of dissipated energy.

Parameters for Separation/Gapping of the Pile from the Soil, and Pinching Hysteretic Behavior of the Pile

One aspect of the effect of lateral loading on pile response which deserves particular attention is the possibility of a gap opening up around the pile near ground level. The proposed model for piles is capable of simulating such a complex geometric nonlinearity. The parameter L_s in Eq. (2) controls the extent of the separation gap of the pile from the soil while the parameter ζ_{s1} controls the range of ζ_s about $\zeta_s=0$, in which the separation occurs, and thus adjusts the "sharpness" of the separation. ζ_{s2} is a constant that controls the shift of the backbone curve on ζ_s axis. The influence of parameter L_s on the shape of a soil reaction-displacement loop is illustrated in Fig. 9. Notice that the larger the parameter L_s, the larger the width of the gap.

Pinching of the hysteretic moment-curvature loops due to opening and closing of cracks is commonly observed in concrete structural elements, such as piles. Pinching behavior is controlled by parameters L_p, ζ_{p1} and ζ_{p2} in the same way that parameters L_s, ζ_{s1} and ζ_{s2} control the separation of the pile from the soil.

Soil Stiffness and Strength Parameters

Under lateral loading, the small-amplitude stiffness k_x ($=P_y/u_y$) in Eq. (1) and the small-amplitude dashpot coefficient c_x in Eq. (3) can be approximated by (Makris and Gazetas, 1992)

$$k_x = 1.2\,E_s \tag{6}$$

and

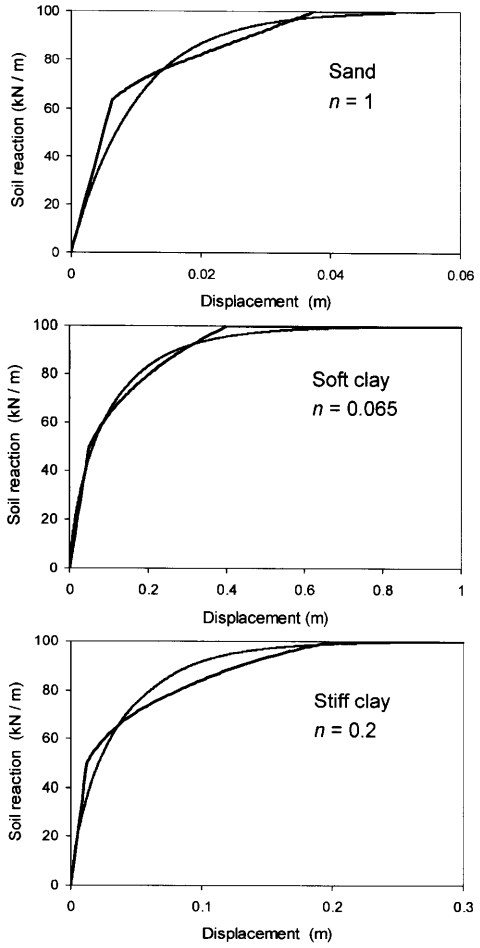

Fig. 5. Comparison of p-y curves computed with the proposed model for piles (smooth lines), and proposed by Reese & Matlock (trilinear line) for sand, soft, and stiff clay respectively

$$c_x = 2\left[1+\frac{3.4}{\pi(1-\nu)}\right]^{1.25}\left(\frac{\pi}{4}\right)^{0.75}\left(\frac{\omega d}{V_s}\right)^{-0.25}\rho_s V_s d \qquad (7)$$

respectively. E_s is the Young's modulus of the soil, ρ_s the soil density, V_s the shear wave velocity of the soil, d the pile diameter, ν the Poisson's ratio of the soil, and ω the cyclic frequency of motion. Note that k_x has units of stiffness per unit length of the pile, and it corresponds to the traditional *'subgrade modulus' multiplied by the diameter, d*, of the pile. Equations (6) and (7) have been derived by matching the dynamic head displacement from Winkler and from dynamic finite element analysis, for a soil Poisson's ratio of $\nu = 0.4$. The reader is referred to the work of Gazetas and Dobry (1984) for more details. For piles in cohesive soils the ultimate soil reaction per unit length of pile can be approximated by the well

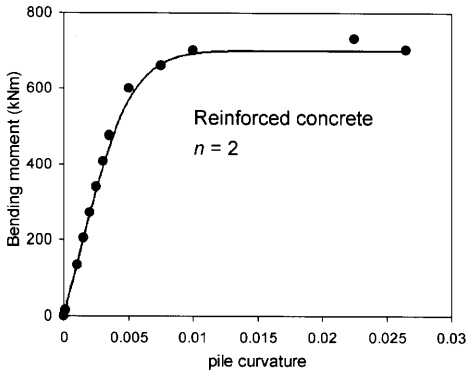

Fig. 6. Comparison of bending moment-curvature monotonic loading curve computed with the proposed model for piles (smooth lines), and derived from a rigorous analysis of the pile cross section (points)

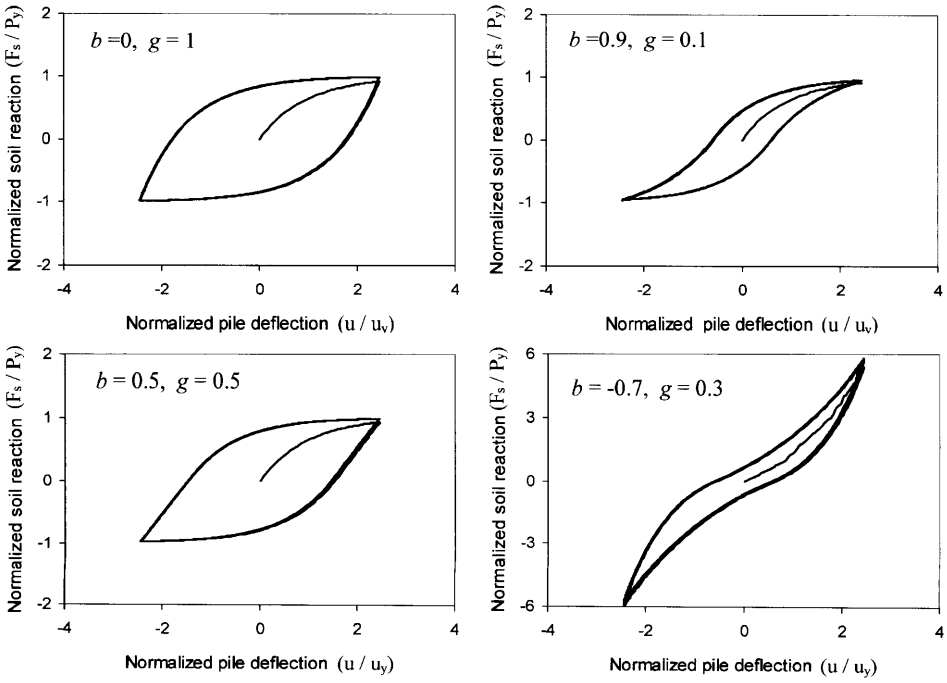

Fig. 7. Hysteretic normalized soil reaction-pile deflection loops for different values of b and g, and $n = 1$: The Masing criterion for unloading-reloading is obtained for $b = 0.5$, $g = 0.5$

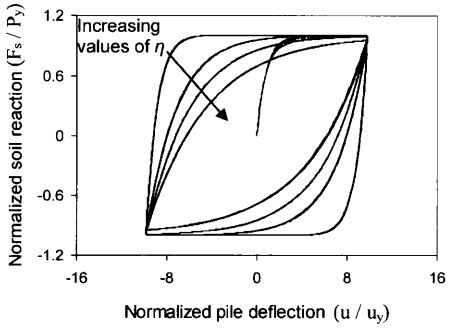

Fig. 8. Effect of parameter η on the stiffness deterioration of force-displacement hysteretic loops

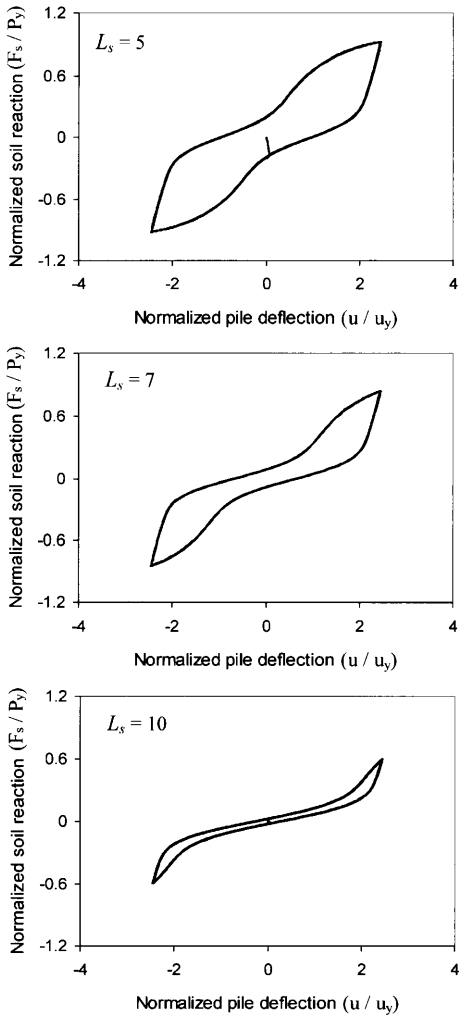

Fig. 9. Normalized soil reaction-pile deflection loops with separation of the pile from the soil computed by BWGG model for piles, for selected values of parameter L_s ($n=1$, $b=0$, $g=1$, $\zeta_{s1}=0.2$)

known expression;

$$P_y=\lambda_1 S_u d \tag{8}$$

where S_u is the soil undrained shear strength, and λ_1 varies from 9 to 12, depending on the friction ratio f_s/S_u at the pile-soil interface. A value of $\lambda_1=9$ is often used for soft clay, while $\lambda_1=11$ is more appropriate for stiff clay. At shallow depths, the plane strain assumption of Eq. (8) is inappropriate because of the non-zero vertical deformation of the soil during lateral motion of the pile. The following formulation has been proposed for P_y near the surface (Matlock, 1970);

$$P_y=\left(\lambda_2+\frac{\sigma'_v}{S_u}+J\frac{z}{d}\right)S_u d, \quad z<\frac{(\lambda_1-\lambda_2)d}{\frac{\gamma'_s d}{S_u}+J} \tag{9}$$

where σ'_v is the vertical effective stress, and γ'_s the effective specific weight of the soil, and λ_2 and J are dimensionless quantities. Broms (1964) proposed a value of $\lambda_2=2$, whereas Matlock (1970) used $\lambda_2=3$. Matlock (1970) stated that the value of J was determined experimentally to be 0.5 for soft clay and about 0.25 for medium clay, whereas Reese (1975) suggested a value of $J=2.83$ for all types of clay. For piles embedded in cohesionless soils, Broms (1964) proposed an analytical expression for the ultimate soil reaction:

$$P_y=3\gamma'_s d\tan^2\left(45°+\frac{\phi}{2}\right)z \tag{10}$$

where φ is the angle of friction. Equation (10) is very often preferred in practice among other more rigorous expressions for its simplicity and compatibility with experimental results.

Parameters for Radiation Damping (Viscoplastic Approach)

Under dynamic loading, part of the input energy is dissipated through soil hysteresis in the vicinity of the pile and part is radiated outward away from the pile. These two types of damping (hysteretic and radiation) are fully coupled, though usually they are modeled as separate. Increasing the amplitude of the applied load, increases soil nonlinearity and reduces radiation damping (e.g., Gazetas and Dobry, 1984). In fact radiation of wave energy is proportional to the S-wave velocity of the soil, and with increasing nonlinearity this velocity will decrease in the neighborhood of the pile. In addition, the lateral inhomogeneity that is effectively created (secant wave velocity decreases continuously towards the pile-soil interface) leads to continuous reflections of the radial propagating waves, thereby further undermining radiation damping. Separation of the pile from the soil also has a significant effect in reducing radiation damping.

The proposed model could capture this coupling of hysteretic with radiation damping with a certain degree of realism. As it is shown in Eq. (3) the dashpot force is expressed as a function of the first derivative of ζ_s with respect to pile deflection u, which controls the soil hysteretic response around the pile. The viscoplastic parameter c_s, controlling the influence of soil hysteretic response on radiation damping, ranges from 0 to 0.5. When $c_s=0$, then Eq. (3) reduces to linear (small-amplitude) dashpot equation.

$$F_d=c_x\frac{\partial u}{\partial t} \tag{11}$$

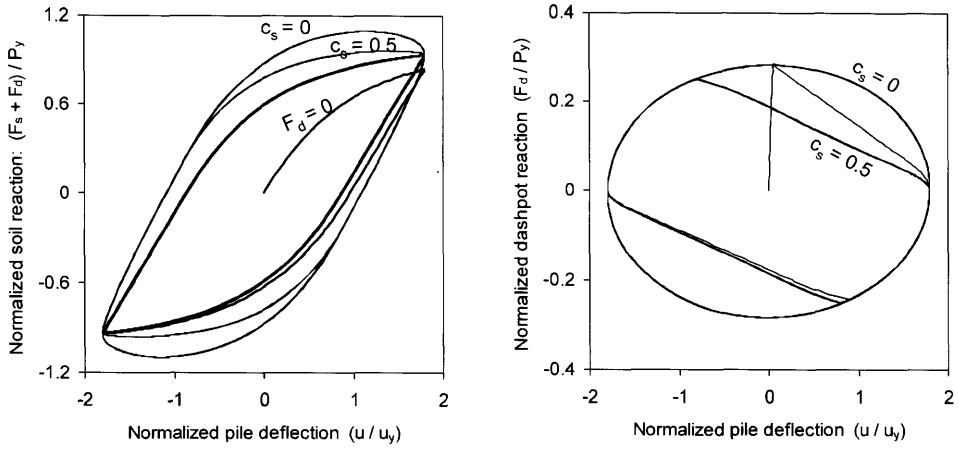

Fig. 10. Left: Normalized soil reaction-pile deflection loops for selected values of viscoplastic parameter c_s computed with the BWGG model for piles, Right: The associated viscoelastic ($c_s = 0$) and viscoplastic ($c_s = 0.5$) component of soil pressure (dashpot reaction)

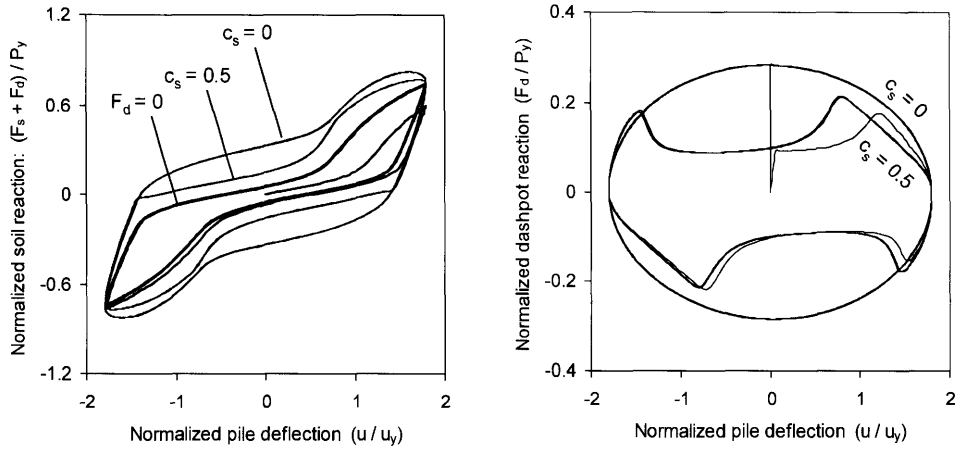

Fig. 11. Left: Normalized soil reaction-pile deflection loops with gapping effect, for selected values of viscoplastic parameter c_s computed with the BWGG model for piles, Right: The associated viscoelastic ($c_s = 0$) and viscoplastic ($c_s = 0.5$) component of soil pressure (dashpot reaction)

The larger the value of c_s the more representative the dashpot is for soil-pile interaction when high-frequency waves are emitted from the pile periphery. Figure 10 shows typical soil reaction (normalized to the ultimate soil reaction P_y) vs pile deflection (normalized to the yield displacement u_y) loops computed with BWGG model for piles, for different values of parameter c_s. The associated viscoplastic components are also presented in this figure. Similar curves for soil reaction with gapping effect are depicted in Fig. 11. Note the profound reduction in radiation damping either when gapping occurs, or when the ultimate soil reaction is being reached. Paradoxically the opposite is observed when a viscoelastic approach for the radiation damping is adopted ($c_s = 0$).

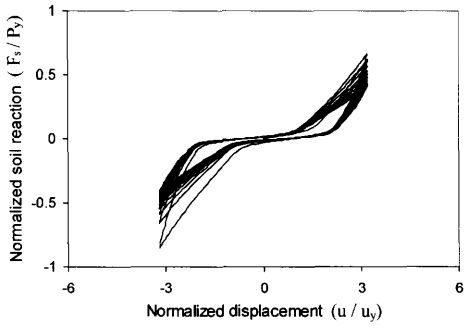

Fig. 12. Hysteretic component of a typical soil reaction on a pile in stiff clay with gapping effect and strength deterioration, computed with the proposed model for piles

Model Capabilities

As it was shown through the discussion of the role of the key model parameters, the BWGG model for piles allows considerable flexibility in representing complex nonlinear features of cyclic behavior of pile-soil systems. It can reproduce a variety of moment-curvature or force-displacement hysteretic loops. As an example, Fig. 12 illustrates a soil reaction-displacement loop computed with the BWGG model for a pile embedded in stiff clay and experiencing gapping and degrading behavior with cyclic loading. Moreover, Fig. 13 depicts moment-curva-

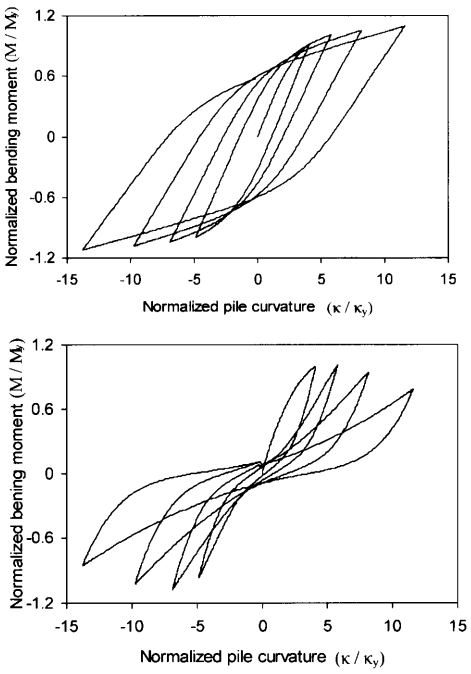

Fig. 13. Moment-curvature loop of a well-reinforced (top), and a poorly reinforced concrete pile section (bottom), computed with the proposed model for piles

ture loops for a poorly-reinforced and a well-reinforced concrete pile sections, computed with the proposed model for piles. Note the flexibility of the model in capturing the strength deterioration and pinching behaviour of the first case, and the strains hardening behaviour of the second case. It shall be noted here that Figs. 12 and 13 aim at a quantitative demonstration of the potential capabilities of the proposed model. The methodology of calibrating the model parameters related to those hysteretic loops, is beyond the scope of this article.

NUMERICAL MODELING OF PILE RESPONSE TO STATIC AND CYCLIC LOADING

The problem studied is that of a single pile embedded in a layered soil and subjected to lateral motion. The pile is considered as a beam with cross-sectional area, A_p and mass density ρ_p. The bending moment of a pile section is a nonlinear hysteretic function of its curvature. The soil-pile interface is modeled as a Winkler foundation, with continuously distributed nonlinear springs and viscoplastic dashpots, as sketched in Fig. 14. Dynamic equilibrium of the pile gives

$$\frac{\partial^2 M(z,t)}{\partial z^2} + \rho_p A_p(z) \frac{\partial^2 u(z,t)}{\partial t^2} + F_s(z,t) + F_d(z,t) = 0 \quad (12)$$

where z is the spatial coordinate (depth) along the pile, and t is the time. M is the pile bending moment given by Eq. (4), and F_s and F_d are the spring and dashpot reactions on the pile given by Eqs. (1) and (3), respectively.

An explicit finite difference method is used for the

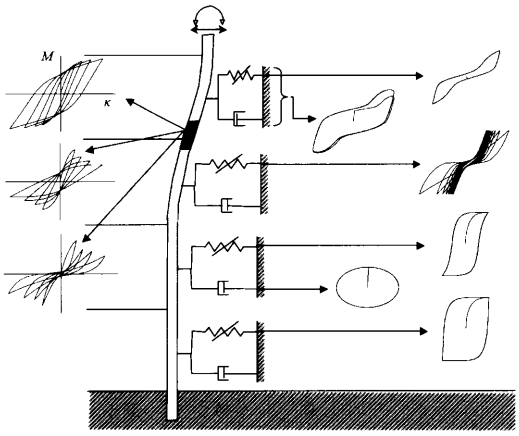

Fig. 14. Schematic illustration of dynamic nonlinear pile-soil interaction: The BWGG model for piles

solution of the system of Eq. (12) coupled with Eqs. (1) through (5), by considering the variation of pile and soil properties along the pile length. Head and tip boundary conditions are appropriately taken into account. The BWGG model for piles is incorporated into a computer code named NL-DYAP for the nonlinear analysis of single piles under lateral loading, Gerolymos (2002).

CASE STUDIES: FULL SCALE EXPERIMENTAL PILE RESPONSE TO STATIC AND DYNAMIC LOADING

The capability of the model is demonstrated by predicting the measured data of two full-scale experiments of single piles subjected to lateral monotonic and cyclic loading.

Case Study 1: Monotonic Response of Pile in Soft Clay

Matlock (1970) presented results from lateral-load tests employing a steel pipe pile that was 0.32 m in diameter, with a wall thickness of 12.7 mm, and a length of 12.8 m. The yield bending moment was computed to be 231 kNm, and the bending moment capacity was computed to be 304 kNm. The pile was driven into clays near Lake Austin, in Texas, that are slightly overconsolidated by desiccation, slightly fissured, and classified as CH. The undrained shear strength, measured with a field vane, was found to be almost constant with depth, about 38 kPa. The soil properties and pile characteristics are illustrated in Fig. 15. The pile was subjected to a force-controlled loading applied at its head, 6.35 cm above groundline (Reese and Van Impe, 2001).

The monotonic loading parameter, $n_s = 0.065$, of the proposed model was calibrated by fitting the *p-y* curves for soft clay with free water surface proposed by Matlock (1970), as was already shown in Fig. 5. n_p (parameter for bending moment-curvature monotonic loading curve) is taken as being equal to 3. The Young's soil modulus of elasticity used for the calculation of the small-amplitude spring stiffness, Eq. (6), is estimated from empirical correlations with the undrained shear strength.

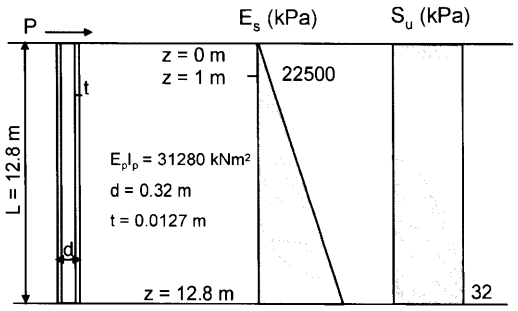

Fig. 15. Soil properties and pile characteristics of the in-situ pile load test carried out by Matlock (1970)

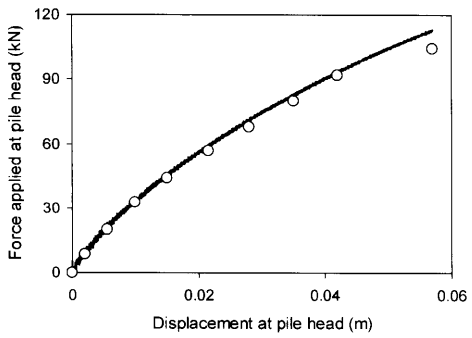

Fig. 16. Comparison of computed head force-displacement curve (solid line) with the experimental data (circles) from Matlock (1970)

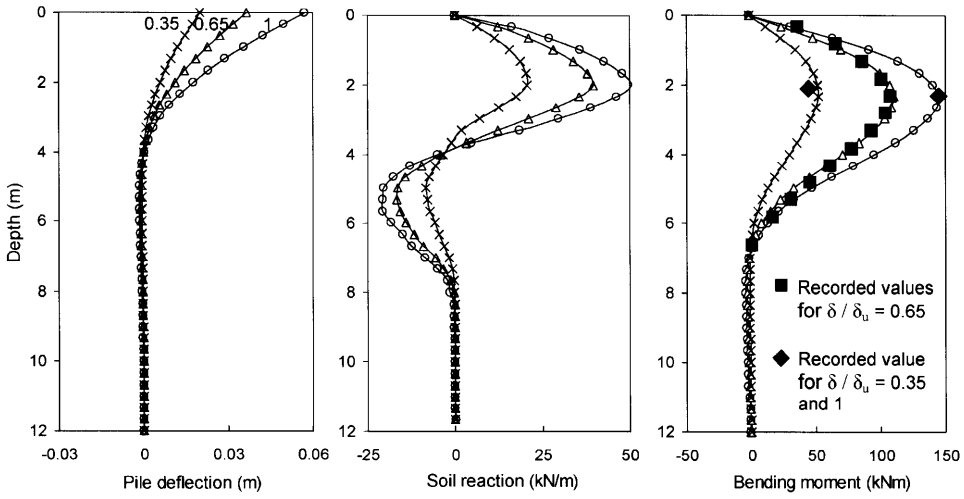

Fig. 17. Computed pile deflection, soil reaction, and bending moments profiles at selected loading levels corresponding to the full scale pile load test carried out by Matlock (1970): The experimental data for bending moment are plotted with bold squares

Figure 16 compares the computed versus recorded force-displacement curve at the pile head. The resulting bending moment profiles computed for the different stages of loading are compared with the moment recorded at the end of loading in Fig. 17. The comparisons are very satisfactory. Also portrayed in Fig. 17 are the computed distributions with depth of pile deflection and soil reaction at the same stages of loading. The variable parameter in these plots (indicating the stages of loading) is the ratio of the applied displacement to the ultimate head displacement (=0.057 m). Note that the plastification of clay surrounding the pile begins at the very early stage of loading, causing a softened pile response despite the appreciable initial stiffness of the soil.

Case Study 2: Cyclic Response of Pile in Saturated Silty Sand

Ting (1987) conducted a detailed study of the dynamic response of a cylindrical steel pile driven into a dense, saturated, silty fine sand located at Seal Beach, California. Details on the experimental setup can be found in the original paper. The soil Young's modulus is assumed to be constant, 6 MPa, for a depth of 2 m; it then increases linearly with depth having a value of 30 MPa at depth of

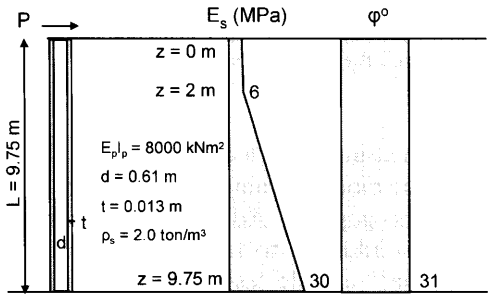

Fig. 18. Soil properties and pile characteristics of the in-situ dynamic load test contacted by Ting et al., 1987

9.75 m (location of the pile tip). The angle of internal friction is reported as $\varphi = 31°$. The soil properties and pile characteristics are illustrated in Fig. 18.

By best fitting the "experimental" *p-y* curves for sand with free water surface proposed by Matlock (1970), as already shown in Fig. 5, the optimum monotonic loading parameter $n_s \approx 1$ was obtained. A value of $n_p = 3$ was adopted for the monotonic pile bending moment-curvature loading curve. It is reported (Reese and Van Impe, 2001) that separation and gapping occurred during

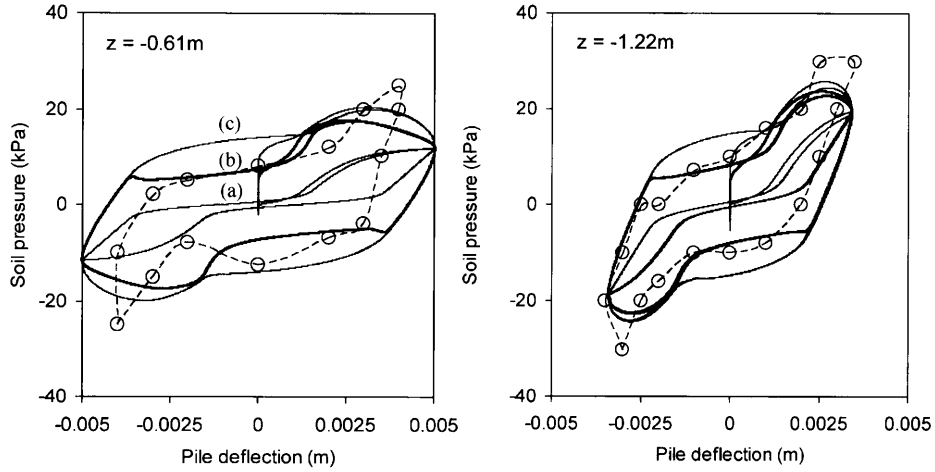

Fig. 19. Comparison of predicted dynamic soil reaction (solid lines) at frequency $f = 2.1$ Hz and at depths of -0.61 m and -1.22 m respectively, against the recorded data from Ting (1987): The computed soil reactions are (a) the purely hysteretic component, (b) the resultant soil pressure with viscoplastic radiation damping and (c) the resultant soil pressure with viscoelastic radiation damping

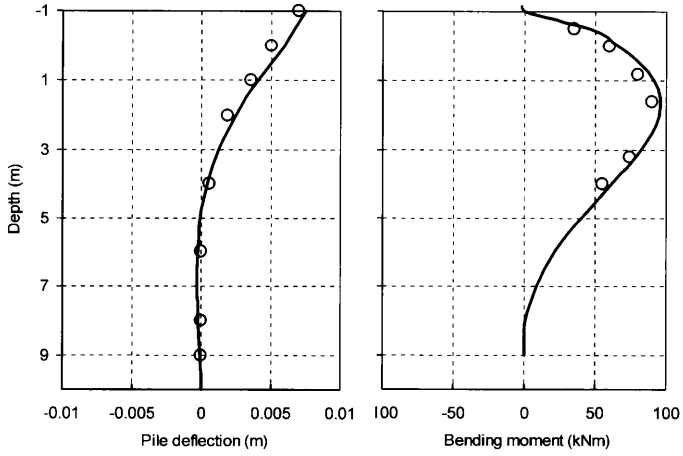

Fig. 20. Comparison of computed pile deflection and bending moment distributions (solid line) with the experimental data of Ting (1987): The applied force on the pile head is 11 kN

loading. The measured depth of the gap was about 1.5 m; the choice of the model parameters L_s, ζ_{s1} and ζ_{s2} was such as to capture this gapping. Admittedly, utilizing the extra information (in addition to the local *p-y* curves) makes our "prediction" a little less "blind" than a genuine (Class A) prediction as would be the case in a practical design application.

Figure 19 compares the computed static deflections and bending-moments profiles, with the experimental data points. The agreement is indeed very good, which attests both to the realism of the *p-y* curves themselves *and* to the capability of our model to reproduce them; and as already mentioned, the information on the depth of the (actual) gap has, undeniably, also helped.

To further investigate the capabilities of the model, the resultant soil pressure is computed at different depths. Figure 20 compares the predicted soil pressure-vs-pile-deflection loops against the recorded data at two different depths. Evidently, the model can capture with reasonable accuracy the consequences of gapping. The success of this comparison is equally encouraging in view of the well known difficulty to predict in detail simultaneously both stiffness and damping at this local level.

INELASTIC SOIL-PILE INTERACTION UNDER LATERAL MONOTONIC LOADING

The developed model is further utilized in studying the problem sketched in Fig. 21: a reinforced concrete pile of length $L = 20$ m and diameter $d = 1$ m, embedded in a cohesionless soil, undergoes lateral loading up to failure. The pile is considered to be fixed at its head with no rotation allowed, while a small length of 0.5 m protrudes above the ground surface. The Young's modulus and the internal friction of the soil are $E_s = 33$ MPa and $\varphi = 30°$, respectively. The bending moment capacity of the pile section is $M_u = 2000$ kNm. The pile is subjected to a controlled lateral monotonic displacement at its head until complete "failure".

Three cases are considered: (a) Nonlinear response is

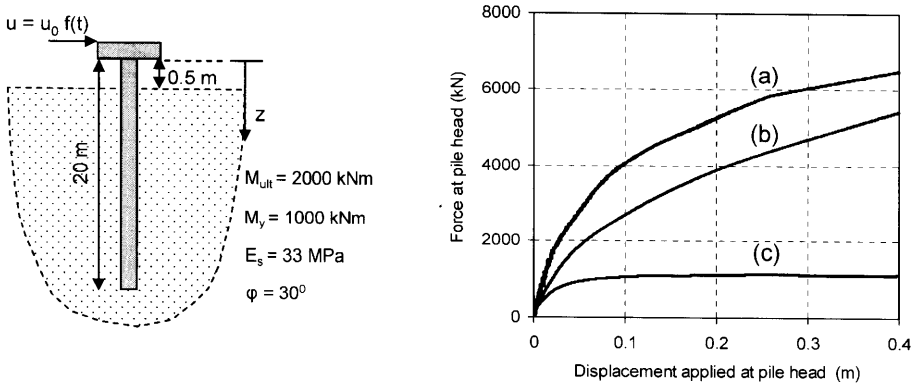

Fig. 21. The studied problem and the computed pile head monotonic force-displacement curves referring to: (a) nonlinearity in the pile only, (b) nonlinearity in the soil only and (c) nonlinearity in both soil and pile

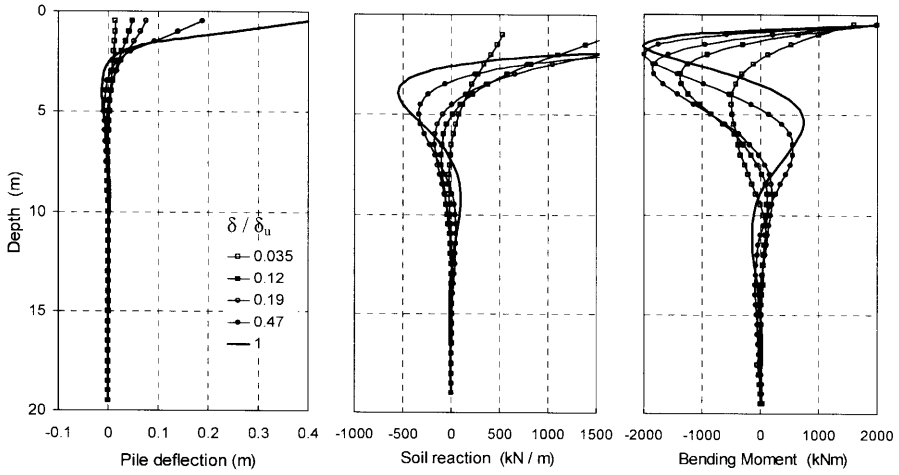

Fig. 22. Pile deflection, soil reaction, and bending moments profiles at different stages of loading, for the first case (nonlinearity in the pile only)

restricted in the pile only, while the soil remains elastic, (b) nonlinear response is allowed for only in the soil, and (c) nonlinear response applied to both the pile and the soil. For all the three cases the ductility capacity (in terms of curvature) of the pile is considered to be unlimited.

The predicted force-displacement curves at the head of the pile for the three cases are illustrated in Fig. 21.

It appears that a dramatic reduction in ultimate capacity occurs when both pile and soil develop plastic deformation. The details of the computed pile deflection, soil reaction, and bending moment distributions at different stages of loading are presented in Fig. 22, Fig. 23, and Fig. 24 for the first, second and third case, respectively. The parameter is the ratio δ/δ_u, of the applied lateral displacement to the maximum head displacement; it is given values from 0.035 (almost linear case) to 1 (ultimate load).

The following observations are worthy of note in these figures:

(a) Regarding the first case (Fig. 22), where only nonlinearity of the pile is allowed to occur, the formation of the first plastic hinge at the pile head ($M_u = 2000$ kNm), takes place at an early stage of loading, before even the applied pile head displacement reaches 4 cm (or $\delta/\delta_u \approx 0.10$). The in-depth local maximum of (negative) bending moment initially appears at the depth of about 4.5 m. With increasing load this local maximum is being shifted upwards, until the development of a second plastic hinge ($M_u = 2000$ kNm) at the depth of about 3 m, for a head displacement of 8 cm (or $\delta/\delta_u \approx 0.19$). With further increases in head displacement, this second plastic hinge is also being shifted upwards to a depth of 1.5 m, which is, approaching the first plastic hinge. It is worthy of note that no catastrophic failure mechanism is created, despite the formation of the second plastic hinge (at a pile head force of 4000 kN). This is because in the analysis, the piles capacity for continuous increase even beyond the maximum imposed pile head displacement (=0.40 m). This of course is only an artefact of assumed unlimited ductility capacity of the pile which in conjunction with the soil confinement allows a redistribution of pile bending moments to occur.

(b) Regarding the second case where only the soil is allowed to yield, Fig. 23 shows that:

- The ultimate soil reaction, theoretically being equal to $p_{ult} \approx 3\, K_p\, \gamma_s\, z\, d$ (where K_p is the Rankine

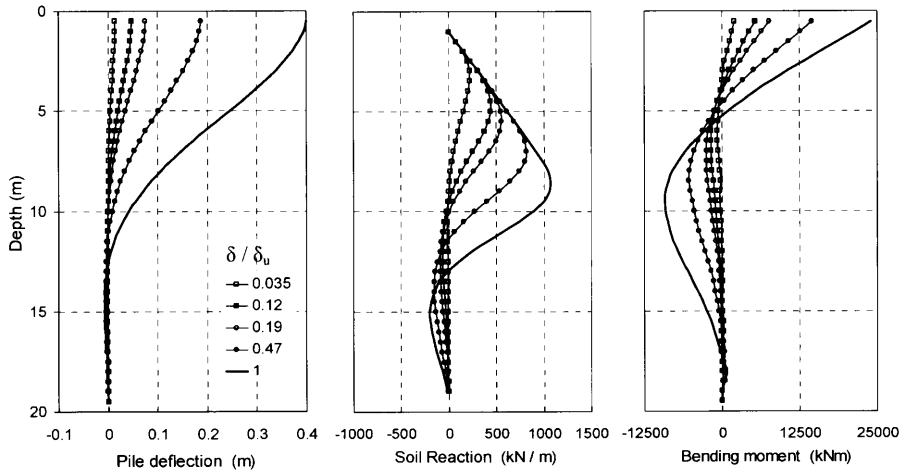

Fig. 23. Pile deflection, soil reaction, and bending moments profiles at different stages of loading, for the first case (nonlinearity in the soil only)

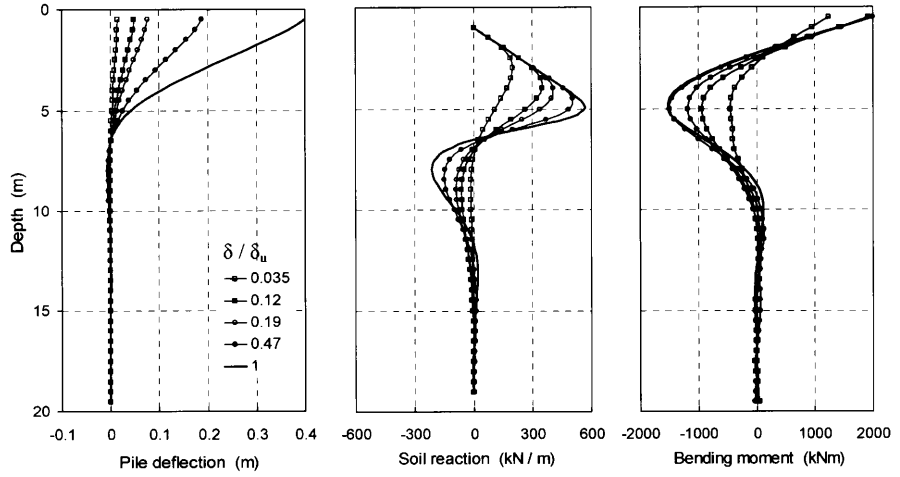

Fig. 24. Pile deflection, soil reaction, and bending moments profiles at different stages of loading, for the first case (nonlinearity in both pile and soil)

coefficient of passive earth pressure), is mobilized from the early stages of loading, but of course initially only down to very small depths from the surface (notice the linearly increasing portion of soil reaction). Soil yielding extends progressively to greater depths as the load increases. At the ultimate condition, $(\delta/\delta_u = 1$, soil yielding has reached down to a depth of about 7.5 m, with a soil reaction of 1000 kN/m—a value falling within 10% of the idealized theoretical value: $p_{ult} \cong 3 \times 3 \times 16 \times 7.5 \approx 1080$ kN/m (e.g., Poulos and Davis, 1980).

- The assumed perfect elasticity of the pile leads to exceedingly high bending moments at the fixed head position; such moments will exceed the ultimate capacity of even the most heavily reinforced concrete pile of $d = 1$ m. Nevertheless, since nonlinearity of the pile is not taken into account, the ultimate lateral capacity will be reached only when soil plastification along the whole pile length will take place. Hence the undiminished ascend of the F-δ curve (a) of Fig. 21.

(c) The lateral capacity of the pile in the third case (nonlinearity in both pile and soil) is computed to reach a mere 1150 kN, at pile head displacement of only 0.10 m. At this relatively early stage of loading not only a fully plastic hinge $(M = M_{ult} = 2000$ kNm/m) forms at the pile head but yielding of the pile cross-section $(M \approx M_{yield} \approx 1000$ kNm) also develops at a depth of about 5 m, as shown in Fig. 24. The development of the second "partial" plastic hinge at the depth of 5 m is not associated with the full ultimate bending capacity at this point, even at very large pile deflections. This is because the soil plastification propagates rapidly downward with increasing pile head displacement, (notice the increasing depth of the linear p_{ult} soil reaction) and passes the depth of 5 m before the bending moment had a chance to reach its maximum value at this point. This local maximum of bending moment is finally stabilized at 1500 kNm.

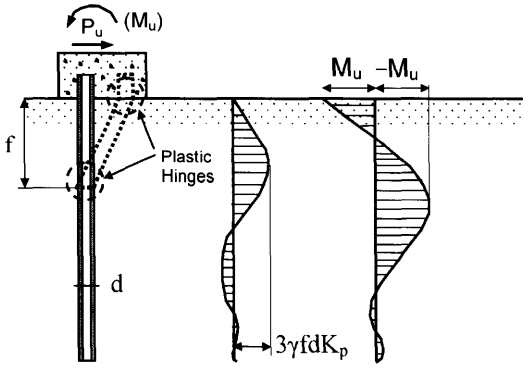

Fig. 25. Failure mode of a fixed head pile in cohesionless soil, with the corresponding soil reaction and bending moment profiles (after Broms, 1964): K_p = the Rankine coefficient of passive earth pressure: The qualitative agreement with the results of Fig. 24 for the largest applied load is evident

Observe that the displacement profile retains a nearly triangular shape with maximum value at the surface and zero value almost at $z = 5$ m. Below this depth the pile remains idle to reminiscent of the "active" length of piles under elastic conditions (Randolph, 1979; Gazetas and Dobry, 1984).

Comparison with Broms Theory of Pile Lateral Capacity

Broms (1964) ingenious theory of pile lateral capacity is still very often used in practice because of its simplicity and rationality. It is an ultimate capacity method, in that both soil and pile develop their full inelastic response. The fundamental assumption underlying the method is that the pile movements are sufficient to fully mobilize the plastic capacities everywhere, and that the elastic deformations are ignored.

The failure mode of a fixed head long pile in cohesionless soil along with the corresponding soil reaction and bending moment profiles, is illustrated in Fig. 25. According to Broms the lateral capacity is reached when the moment from soil reactions balances the summation of the ultimate bending moment at pile head and at the depth where the maximum soil resistance develops. The qualitative similarity of Broms' Fig. 25 with our Fig. 24 is striking. Applying Broms theory to our problem, the ultimate capacity of the pile is obtained as 1380 kN. As expected this estimate overpredicts the value of 1150 kN computed with the proposed model for piles. This is attributed to the fact that, Broms theory does not account for any soil-pile interaction and the formation of the second plastic hinge is always associated with ultimate bending moment in the case of a large pile. In other words, the "inability" of the pile in our analysis to develop a second plastic hinge when extensive soil plastification takes place, largely makes the small difference between the two methods. This attests to the realism of the prediction of the developed BWGG model.

CONCLUSIONS

A beam on Winkler foundation analysis is presented for laterally located piles. Both piles and soil are treated as nonlinear-inelastic materials. To model the nonlinear reaction of the soil with realism we develop the "*BWGG interaction springs and dashpots*" model, which can capture such effects as: soil failure, separation and gapping of the pile from the soil, radiation damping, and loss of strength and stiffness due to degradation and pore-water pressure generation. The coupling of hysteretic and radiation damping is also modeled in a realistically simplified way. The modeling of structural pile inelasticity is versatile, and can treat from well-reinforced to poorly-reinforced concrete sections. Although some guidelines are drawn regarding the calibration of the model parameters and their relation with the physical/geometric characteristics of the soil and the pile, as well as with results from experimental tests, identification and complete calibration of the model parameters is beyond the scope of this paper. The model is shown to be capable of reproducing complicated experimental results of pile load tests, both static and cyclic. The model was utilized to compute the nonlinear response of a pile embedded in cohesionless soil when subjected to lateral monotonic loading. Three cases were studied: (a) nonlinear response for the soil only, (b) nonlinear response for the pile only, and (c) nonlinear response of both pile and soil. The results are in accord with the venerable Broms (1964) theory of ultimate pile lateral capacity.

REFERENCES

1) Baber, T. T. and Noori, M. N. (1985): Random vibration of degrading systems with pinching hysteresis, *J. Engrg. Mech. Div.*, ASCE, **III**(8), 1010–1026.
2) Baber, T. T. and Wen, Y.-K. (1981): Random vibration of hysteretic degrading systems, *J. Engrg. Mech.*, ASCE, **107**, 1069–1087.
3) Badoni, D. and Makris, N. (1995): Nonlinear response of single piles under lateral inertial and seismic loads, *Soil Dynamics and Earthquake Engineering*, **15**, 29–43.
4) Bouc, R. (1971): Modele mathematique d' hysteresis, *Acustica*, **21**, 16–25 (in French).
5) Broms, B. B. (1964a): Lateral resistance of piles in cohesionless soils, *J. Soil Mech. Found. Div.*, ASCE, 1964, **90**(SM3), 123–56.
6) Broms, B. B. (1964b): Lateral resistance of piles in cohesive soils, *J Soil Mech. Found. Div.*, ASCE, 1964, **90**(SM2), 27–63.
7) Gazetas, G. and Dobry, R. (1984a): Horizontal response of piles in layered soils, *J. Engrg. Mech.*, ASCE, **110**, 20–40.
8) Gazetas, G. and Dobry, R. (1984b): Simple radiation damping model for piles and footings, *J. Engrg. Mech.*, ASCE, **110**, 937–956.
9) Gerolymos, N. (2002) Constitutive model for static and dynamic response of soil, soil-pile, and soil-caisson, *Ph. D. dissertation*, National Technical University, Athens (in Greek).
10) Gerolymos, N. and Gazetas, G. (2004): Constitutive model for 1-D cyclic soil behaviour applied to seismic analysis of layered deposits, *Soils and Foundations*, **45**(3), 147–159.
11) Kishida, H., Suzuki, Y. and Nakai, S. (1985): Behavior of a pile under horizontal cyclic loading, *Proc. 11th ICSMFE, San Francisco*, **3**, 1413–16.
12) Makris, N. and Gazetas, G. (1992): Dynamic pile-soil-pile interaction. Part II: Lateral and seismic response, *Earthquake Engineering Structural Dynamics*, **21**, 145–62.

13) Matlock, H. (1970): Correlations for design of laterally loaded piles in soft clay, Paper No. OTC 1204, *Proc. 2nd Annual Offshore Technology Conference*, Houston, Texas, **1**, 577–594.
14) Michaelides, O., Gazetas, G., Bouckovalas, G. and Chrysikou, E. (1998): Approximate non-linear dynamic axial response of piles, *Geotechnique*, **XLVIII**, 33–54.
15) Poulos, H. G. and Davis, E. H. (1980): *Pile Foundation Analysis and Design*, John Wiley & Sons.
16) Poulos, H. G., Carter, J. P. and Small, J. C. (2001): Foundations and retaining structures-research and practice, *Proc. 15th ICSMGE*, Istanbul, **4**.
17) Priestley, M. J. N., Seible, F. and Calvi, G. M. (1996): *Seismic Design and Retrofit of Bridges*, John Wiley and Sons, Inc., New York.
18) Randolph, M. F. (1981): The response of flexible piles to lateral loading, *Geotechnique*, **31**(2), 247–259.
19) Randolph, M. F. (2003): Science and empiricism in pile foundation design, *Rankine Lecture, Geotechnique*, **53**(10), 847–875.
20) Reese, L. C., Cox, W. R. and Koop, F. D. (1974): Analysis of laterally loaded piles in sand, Paper No. OTC 2080, *Proc. 5th Annual Offshore Technology Conference*, Houston, Texas, 1974, **II**, 473–485.
21) Reese, L. C., Cox, W. R. and Koop, F. D. (1975): Field testing and analysis of laterally loaded piles in stiff clay, Paper No. OTC 2312, *Proc. 7th Offshore Technology Conference*, Houston, Texas, **II**, 672–690.
22) Reese, L. C. and Van Impe, W. F. (2001): *Single Piles and Pile Groups under Lateral Loading*, A. A. Balkema.
23) Sastry, V. V. R. N. and Meyerhof, G. G. (1999): Flexible piles in layered soil under eccentric and inclined loads, *Soils and Foundations*, **33**(1), 11–20.
24) Sivaselvan, M. V. and Reinhorn, A. M. (2000): Hysteretic models for deteriorating inelastic structures, *J. Engrg. Mech.*, **126**(6), 633–640.
25) Tabesh, A. and Poulos, H. G. (2001): The effects of soil yielding on seismic response of single piles, *Soils and Foundations*, **41**(3), 1–16.
26) Tassios, Th., Moretti, M. and Bezas, A. (1996): On the behavior and ductility of reinforced concrete coupling beams of shear walls, *ACI Structural J.*, **93**(6), November-December.
27) Ting, J. M. (1987): Full-scale cyclic dynamic lateral pile responses, *J. Geotech. Engrg.*, ASCE, **113**, 30–45.
28) Trochanis, A., Bielak, J. and Christiano, P. (1994): Simplified model for analysis of one or two piles, *J. Engrg. Mech.*, ASCE, **120**, 308–29.
29) Wakai, A., Gose, Sh. and Ugai, K. (1999): 3-D elasto-plastic finite element analyses of pile foundations subjected to lateral loading, *Soils and Foundations*, **39**(1), 97–111.
30) Wen, Y.-K. (1976): Method for random vibration of hysteretic systems, *J. Engrg. Mech.*, ASCE, **102**, 249–263.
31) Wu, B., Broms, B. and Choa, V. (1998): Design of laterally loaded piles in cohesive soils using *p-y* curves, *Soils and Foundations*, **38**(2), 17–26.